Calibration-independent Atomic Force Microscopy

Carolina Pimenta-Lopes[*,#], Carmen Suay-Corredera*, Diana Velázquez-Carreras, David Sánchez-Ortiz, Jorge Alegre-Cebollada*

Centro Nacional de Investigaciones Cardiovasculares Carlos III (CNIC), 28029 Madrid, Spain

*equal contribution
[#]current address: Department of Physiological Sciences, University of Barcelona, Spain
Correspondence to Jorge Alegre-Cebollada: jalegre@cnic.es

ABSTRACT

Atomic Force Microscopy (AFM) is the technique of choice to measure mechanical properties of molecules, cells, tissues and materials at the nano and micro scales. However, unavoidable calibration errors of AFM make it cumbersome to quantify modulation of mechanics. Here, we show that concurrent AFM measurements enable relative mechanical characterization with an accuracy that is independent of calibration uncertainty. To demonstrate calibration-independent AFM, we have achieved concurrent single-molecule nanomechanical profiling of two different proteins. Using orthogonal fingerprinting strategies to sort individual unfolding events, differences in mechanical unfolding forces can be obtained with a 6-fold improvement in accuracy and a 30-fold increase in throughput. Importantly, the performance of calibration-independent AFM is maintained even when averaging data from multiple, independent experiments.

INTRODUCTION

The development of Atomic Force Microscopy (AFM) has enabled imaging the nanoscale with unprecedented length resolution, revolutionizing nanotechnology, materials science, chemistry and biology [1,2]. AFM is based on the detection of interaction forces between a sample and a microfabricated cantilever, the force probe of the technique. The ability of AFM to measure forces at the nano and micro scales can be exploited to image surface topology, while simultaneously quantifying mechanical parameters such as stiffness, viscoelasticity, and adhesion forces [2-4]. Traditionally, low-scanning speeds have limited the reach of AFM; however, recent developments involving miniaturized cantilevers have achieved imaging at video frame rates, launching the field of high-speed AFM [5]. Due to its force sensitivity down to picoNewtons (pN), AFM is also used in force-spectroscopy mode to examine single-molecule dynamics and ligand-receptor interactions under force [6-8], of relevance for cellular stiffness, mechanosensing and mechanotransduction [9-12].

A key limitation of quantitative AFM stems from uncertain calibration of the spring constant (k_{sc}) of the cantilever, which is needed to determine force values [13]. Different calibration methods to estimate k_{sc} have been developed, differing in their simplicity, damage to the cantilever tip, experimental compatibility and associated uncertainty. Estimates of calibration uncertainty up to 25% are usually reported [14]; however, even higher inaccuracies can result from defects in individual cantilevers, and from unpredictable changes in k_{sc} during experimentation due to material deposition, mechanical drift and wear [6,15].

Force calibration uncertainties in AFM lead to inaccurate quantification of mechanical properties, a situation that is worsened in AFM modes where the elusive geometry of the cantilever tip is required to extract mechanical information [16]. Indeed, comparative AFM studies to characterize mechanical modulation of proteins, materials and cells are challenging, since they necessitate multiple experiments, each one affected by different calibration errors [17,18]. As a result, there is a pressing need to develop methods that can overcome inaccurate AFM calibration [17]. The traditional approach to increase statistical power of AFM mechanical determinations is to repeat experiments, since individual calibration errors are more probable to be averaged out as more experiments are included in the analysis [19]. The drawback is a considerable loss of throughput of the technique.

Theoretically, a manner to overcome calibration errors in comparative AFM studies is to measure the samples concurrently in the same experiment, using the same cantilever and under the same calibration parameters [20-22]. Concurrent measurements would also increase the throughput of AFM since no additional experiments would be needed to compensate for individual calibration errors. Here, we use error propagation analysis, Monte Carlo simulations, protein engineering, and single-molecule force-spectroscopy AFM to understand how calibration errors impact determination of mechanical properties by AFM, and develop orthogonal fingerprinting as a simple and widely applicable strategy for concurrent nanomechanical profiling of proteins under the same calibration parameters. Concurrent measurements lead to drastically improved accuracy and throughput of single-molecule force-spectroscopy AFM. We propose that similar strategies can be easily implemented in other AFM modes to achieve equivalent improvements in performance.

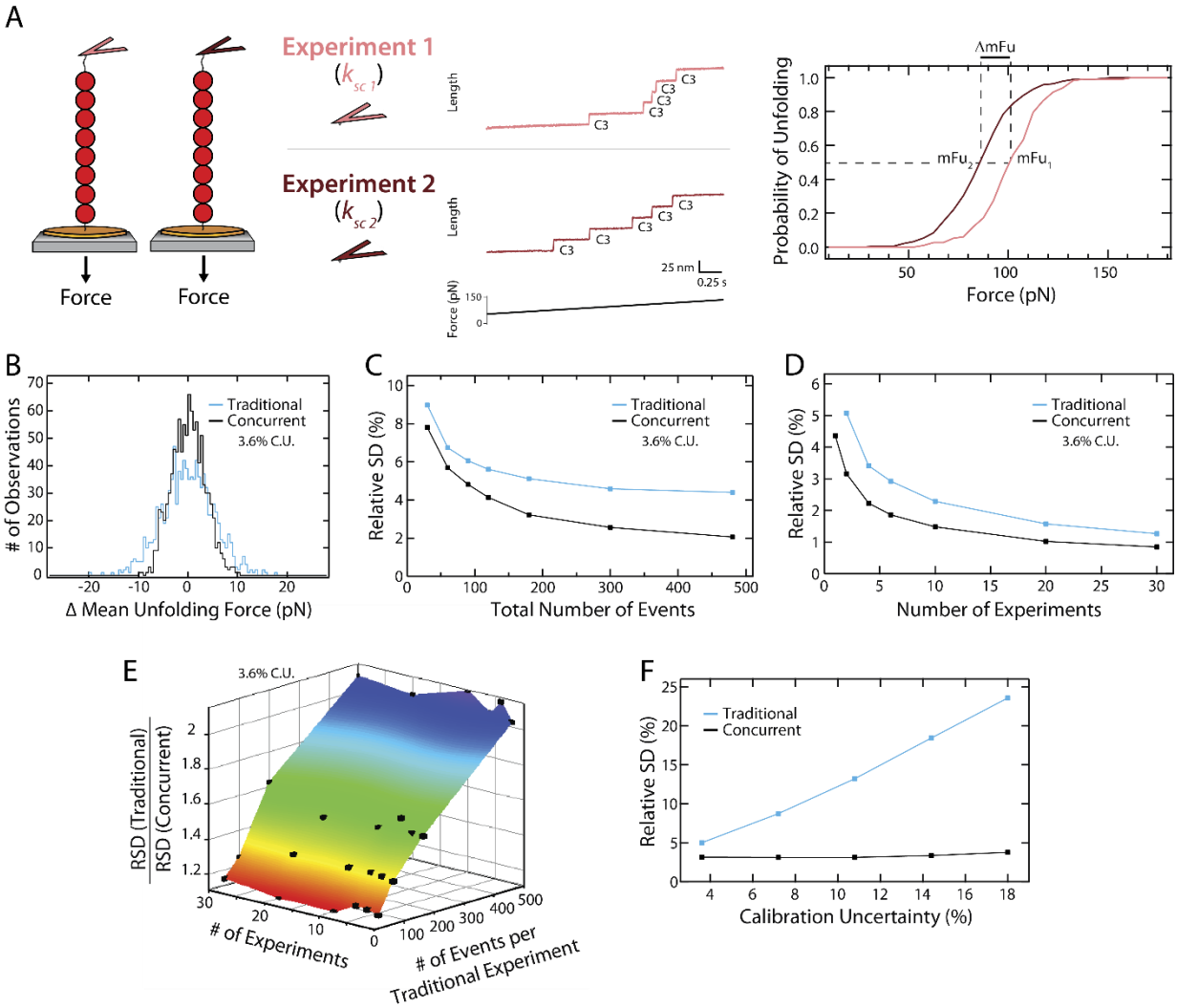

Figure 1. Concurrent mechanical profiling by AFM circumvents inaccurate force calibration. (A) *Left:* Schematic representation of the traditional strategy used to measure mechanical stability of proteins by AFM, in which data are obtained in multiple, independent AFM experiments under different force calibration parameters (see also Supplementary Figure 1). *Middle*: Results from two independent AFM experiments in which a $(C3)_8$ polyprotein is pulled under a 40 pN/s linear increase in force. Due to uncertain calibration of the cantilever's spring constant (k_{sc}), force values are affected by errors that differ between experiments. We show two individual unfolding traces of the $(C3)_8$ polyprotein, in which mechanical unfolding events of individual C3 domains are detected by increases of 24 nm in the length of the polyprotein. *Right*: Experimental cumulative unfolding probability distributions obtained from 117 (Experiment 1) and 191 (Experiment 2) C3 unfolding events. The corresponding mF_u values are 98.7 and 82.9 pN, respectively. **(B)** Distributions of ΔmF_u obtained by Monte Carlo simulations, considering the same total number of experiments and unfolding events for both traditional (blue) and concurrent measurements (black). We considered 2 experiments, 200 total unfolding events per protein, and a 3.6% calibration uncertainty (C.U.) **(C)** Keeping the number of experiments constant (n_{exp}=2), the Relative Standard Deviation (RSD) of the distribution of ΔmF_u decreases with the total number of unfolding events both in traditional (blue) and in concurrent measurements (black). **(D)** Keeping the same number of events per experiment ($n_{events\ per\ experiment}$ = 200, in the traditional approach, and 100 in the concurrent strategy), the RSD of the distribution of ΔmF_u decreases with the number of experiments (blue: traditional strategy; black: concurrent measurements). **(E)** The relative improvement in the RSD of ΔmF_u distributions obtained by the concurrent strategy increases with the number of events per experiment, and remains fairly insensitive to the number of averaged experiments. **(F)** RSD of the distributions of ΔmF_u at increasing calibration uncertainties for the traditional (blue) and the concurrent (black) strategies. The remaining simulation parameters are the same as in panel B. In panels B-F, the number of events per experiment and protein in the concurrent approach was half of the number of events in the traditional strategy so that RSDs were compared between conditions with equal total number of events.

RESULTS

Interexperimental variation of mechanical properties obtained by traditional AFM

To understand how errors in calibration of atomic force microscopes lead to inaccurate determination of mechanical properties, we have measured protein mechanical stability by single-molecule force-spectroscopy AFM [6] (Figure 1A, Supplementary Figure 1). This AFM mode is very well suited to examine propagation of calibration errors since protein unfolding forces are obtained directly from experimental data and do not depend on further modelling or approximations.

We first measured the resistance to mechanical unfolding of the same protein in different, independently calibrated AFM experiments. We produced a polyprotein containing eight repetitions of the C3 domain of human cardiac myosin-binding protein C (Supplementary Figure 2, Supplementary Text 1) and subjected individual $(C3)_8$ polyproteins to a linear increase in force of 40 pN/s using a force-clamp atomic force microscope. Results from two independent experiments are shown in Figure 1A. Mechanical force triggers the stochastic unfolding of individual C3 domains. These unfolding events are detected as 24 nm step increases in the length of the polyprotein (Figure 1A, *middle*; Supplementary Figure 3A). We measured the force at which the unfolding events occur and calculated distributions of unfolding forces [23]. Despite the fact that both distributions are well defined (n > 115 events), the difference in their mean unfolding force (ΔmF_u) is 19% (Figure 1A, right). The magnitude of this interexperimental variation is in agreement with the spread of mF_u values reported in the literature for other proteins [19]. These differences can mask comparable changes in mechanical properties induced by disease-causing mutations [18] or posttranslational modifications [24], which is a key limitation of traditional AFM.

Interexperimental variations in mF_u of proteins are typically interpreted in terms of different errors in the calibration of AFM cantilevers, a procedure that can entail 25% uncertainty [6,13,14,20]. We used Monte Carlo simulations to examine how errors originating from uncertain cantilever calibration propagate to mF_u (See Methods). Briefly, in each simulated experiment we impose an error to the force that is randomly drawn from a normal distribution defined by a Relative Standard Deviation (RSD) that is equal to the considered calibration uncertainty. After definition of the error in force for a cycle, a kinetic Monte Carlo algorithm is used to obtain distributions of unfolding forces for a given number of protein domains subjected to a nominal 40 pN/s increase in force. For each one of the 1,000 cycles of the simulation, we calculate the corresponding ΔmF_u considering a certain number of independent experiments, each one affected by a different calibration error. Simulations return the distribution of ΔmF_u values obtained in the 1,000 cycles. The spread of the distribution, which is a measure of the accuracy of AFM experiments, is quantified by its RSD.

Using our Monte Carlo procedure, we have simulated mechanical protein unfolding under a modest 3.6% force calibration uncertainty. This value is a good estimate of the lowest uncertainty that can be achieved by the thermal fluctuations method, typically used in single-molecule AFM studies (Supplementary Text 2, Supplementary Figure 4) [6]. Figure 1B shows the simulated distribution of ΔmF_u obtained from two independent AFM experiments in which the same protein is probed (200 unfolding events per experiment). It is remarkable that two mean unfolding forces obtained in different cycles can differ by more than 25% (Supplementary Figure 5A). Hence, although conservative, a mere 3.6% inaccuracy in cantilever calibration can explain considerably higher differences in mF_u obtained in traditional AFM experiments.

Accuracy of concurrent AFM experiments is insensitive to calibration uncertainty

It has been argued that concurrent determination of ΔmF_u using a single cantilever, in the same experiment, could minimize the error associated with force calibration [20-22]. However, to the best of our knowledge, the resulting improvement in accuracy has not been quantified. We have used our Monte Carlo simulations to estimate the accuracy achieved by concurrent measurement of mechanical unfolding of two proteins. Considering equal total number of events and experiments, and a 3.6% calibration uncertainty, we find that the RSD of the distribution of ΔmF_u decreases from 5.0% to 3.2% when measurements are taken concurrently (Figure 1B). RSD values are further reduced at higher number of unfolding events, as expected from better definition of the distribution of unfolding forces (Figure 1C, Supplementary Figure 5B). Unexpectedly, averaging multiple concurrent experiments leads to further reductions in RSD, despite the fact that each individual experiment is performed under different calibration parameters (Figure 1D). Increasing the number of events or experiments also results in better accuracy when proteins are probed in traditional, separate experiments (Figure 1 C,D). We find that the relative improvement in accuracy achieved by concurrent over traditional AFM increases with the number of unfolding events per experiment, and remains fairly constant at increasing number of experiments (Figure 1E). Hence, we conclude that averaging independent AFM experiments in which two proteins are probed concurrently retains statistical power, even if those experiments are affected by different calibration errors.

All our simulations in Figure 1B-E were run considering a 3.6% uncertainty in force calibration, which is much smaller than usually reported [6,13,14,20]. Hence, we estimated the RSD of the distribution of ΔmF_u at increasing calibration uncertainties. As expected, higher calibration uncertainties lead to much increased RSD in traditional AFM, whereas the RSD of concurrent distributions remains insensitive to the calibration uncertainty (Figure 1F), even when data from several independent experiments are averaged (Supplementary Figure 6A).

Orthogonal fingerprinting enables concurrent characterization of proteins by AFM

Results in Figure 1D show that under a modest 3.6% uncertainty in force, concurrent AFM measurements can reach the same level of accuracy with 2-4 times less experiments than the traditional approach. Furthermore, at high values of calibration uncertainty, the accuracy of concurrent measurements can be 6 times higher than in the traditional approach (Figure 1F). These remarkable improvements in throughput and accuracy prompted us to design a general strategy to enable concurrent measurement of mechanical properties of proteins.

Having methods to identify single-molecule events is a fundamental requirement of force-spectroscopy AFM. In the case of mechanical characterization of proteins, this need is fulfilled by the use of polyproteins, which provide molecular fingerprints that easily discriminate single-molecule events from spurious, non-specific interactions [25,26] (Supplementary Figure 3). As exemplified in Figure 1A, mechanical unfolding of polyproteins produce repetitive events whose length fingerprints the domain of interest. If two polyproteins are to be measured concurrently in the same experiment, it is imperative that they have different fingerprinting unfolding lengths. Here, we propose a widely applicable manner of achieving such orthogonal fingerprinting (OFP) through the use of heteropolyproteins, in which marker proteins are fused to the proteins of interest [27]. Since OFP identifies proteins through the unfolding length of the marker domains, proteins of interest to be compared in concurrent AFM measurements can have the same unfolding length (e.g. mutant proteins). To test whether heteropolyproteins can be

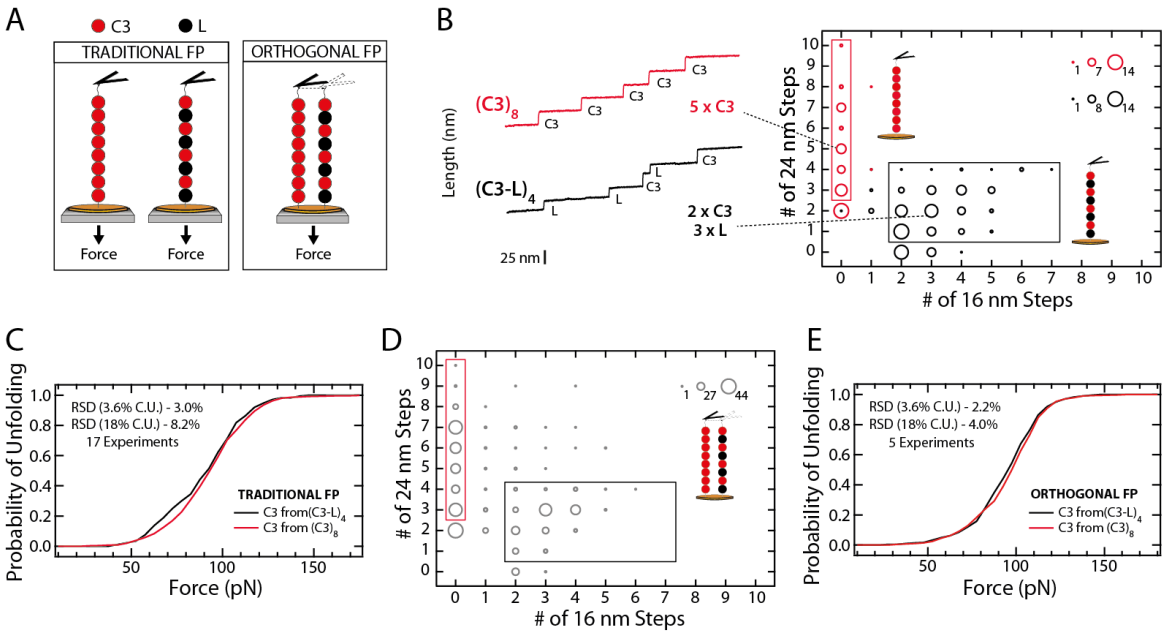

Figure 2. Orthogonal fingerprinting enables concurrent measurement of proteins in AFM. (A) Schematic representation of the traditional and orthogonal fingerprinting (FP) strategies. *Left*: in traditional FP, $(C3)_8$ and $(C3\text{-}L)_4$ are measured in different AFM experiments. *Right*: In orthogonal FP both polyproteins are measured concurrently in the same experiment. **(B)** *Left*: representative unfolding traces of one $(C3)_8$ molecule (red), in which five 24 nm unfolding events are detected, and one $(C3\text{-}L)_4$ polyprotein (black) in which two 24 nm and three 16 nm unfolding events are observed. *Right*: Mechanical unfolding of $(C3)_8$ (red) and $(C3\text{-}L)_4$ (black) were measured in separate experiments. Individual traces were classified according to the number of 16 and 24 nm steps they contain. The plot shows the frequency of the traces that have different combinations of unfolding events, as indicated by the size of the dots. The rectangles represent gating strategies that unequivocally identify traces coming from $(C3)_8$ or $(C3\text{-}L)_4$. **(C)** Experimental cumulative unfolding probability distribution of the C3 domain in the context of $(C3)_8$ (11 experiments, 1334 events, red) and $(C3\text{-}L)_4$ (6 experiments, 177 events, black), following TFP. **(D)** $(C3)_8$ and $(C3\text{-}L)_4$ polyproteins were measured concurrently in the AFM. Resulting traces were classified according to the number of 16 and 24 nm events they have. The plot shows the frequency of the traces that have different combinations of unfolding events, as indicated by the size of the dots. The gating criterion defined in panel B allows the classification of individual traces as resulting from $(C3)_8$ (red rectangle) or $(C3\text{-}L)_4$ (black rectangle). **(E)** Experimental cumulative unfolding probability distribution of the C3 domain in the context of $(C3)_8$ (625 events, red) and (C3-L)4 (311 events, black), resulting from unfolding data obtained in 5 independent OFP experiments. RSD values in the insets of panels C and E are estimated using Monte Carlo simulations that consider extreme values of calibration uncertainty (C.U.) (see also Supplementary Figure 7A). The pulling rate in all experiments was 40 pN/s.

employed to achieve OFP during concurrent measurement of proteins by AFM, we have measured the mechanical stability of the C3 domain in different polyprotein contexts.

We first followed a single-marker strategy using the heteropolyprotein $(C3\text{-}L)_4$ (Figure 2, Supplementary Figure 2 and Supplementary Text 1). In $(C3\text{-}L)_4$, we used protein L as a marker since its unfolding length is different from the one of C3 [19]. Indeed, mechanical unfolding of $(C3\text{-}L)_4$ under a 40 pN/s ramp results in the appearance of 16 and 24 nm steps, which correspond, respectively, to the unfolding of L and C3 domains (Figure 2B, *left*, Supplementary Figure 3B). We selected unfolding traces of $(C3)_8$ and $(C3\text{-}L)_4$, obtained in independent, traditional fingerprinting (TFP) experiments, and classified them according to the number of 16 and 24 nm events they contain. Our results show that a gating criterion of n(16nm) = 0 and n(24nm) > 2 unambiguously identifies traces coming from $(C3)_8$, whereas traces resulting from $(C3\text{-}L)_4$ can be safely assigned when n(16nm) > 1 and 0 < n(24nm) < 5 (Figure 2B, *right*). We analyzed 17 such TFP experiments and obtained distributions of unfolding forces for C3 in the

context of both polyproteins, which we found to be very similar (mF_u = 90. 7 and 88.4 pN for the homo and the heteropolyproteins, respectively, Figure 2C). We used our Monte Carlo simulations to estimate the RSD associated to ΔmF_u that is expected from the actual number of experiments and events obtained (Figure 2C, Supplementary Figure 7A, Supplementary Table 1).

Following validation of the polyprotein gating criterion (Figure 2B), we measured $(C3)_8$ and $(C3\text{-}L)_4$ concurrently in OFP experiments. Single-molecule traces were classified according to the number of 16 and 24 nm steps they contain, and sorted as coming from the $(C3)_8$ or $(C3\text{-}L)_4$ before analysis of unfolding data (Figure 2D). As in the case of TFP experiments, the unfolding probability distributions of C3 in the context of $(C3)_8$ and $(C3\text{-}L)_4$ are very similar (mF_u = 96.3 and 93.4 pN for the homo and the heteropolyproteins, respectively, Figure 2E). However, only 5 OFP experiments were required to reach a lower RSD than in TFP, a 3 times higher speed of data acquisition (Figure 2C,E, Supplementary Figure 7A).

Dual-marker orthogonal fingerprinting overcomes confounding protein dimerization

In the AFM experiments reported in Figures 1 and 2, polyproteins are picked up by the cantilever through non-specific physisorption. Hence, experimental traces can contain different number of unfolding events (Figure 2B). Non-specific protein pickup also leads to the occasional appearance of traces containing more unfolding events than engineered domains in the polyprotein, an effect that results from polyprotein dimerization [28]. For instance, in Figure 2B a few traces with n(24 nm) > 8 are identified when pulling from $(C3)_8$. Comparison of Figures 2B and 2D identifies a new population of events at n(24nm) > 4 and n(16nm) > 1 that appear only when $(C3)_8$ and $(C3\text{-}L)_4$ are measured concurrently in the same experiment, which we interpret as heterodimers between $(C3)_8$ and $(C3\text{-}L)_4$. In the context of OFP, heterodimerization hampers proper assignment of traces, since there is a non-zero probability that some heterodimers are included in the gating region of $(C3\text{-}L)_4$. As a result, a fraction of events coming from $(C3)_8$ could be mistakenly assigned to $(C3\text{-}L)_4$

In general, the degree of protein dimerization in single-molecule AFM is dependent on the particular experimental conditions. Hence, heterodimerization poses a challenge to OFP, whose extent may vary depending on the system to study. However, we hypothesized that difficulties coming from protein dimerization could be overcome by using a second protein marker, since traces originating from dimers would be fingerprinted by the presence of both marker proteins. We chose the protein SUMO1 as a second marker because its unfolding length is different from those ones of C3 and protein L [29]. We engineered the heteropolyprotein $(C3\text{-}SUMO1)_4$ and pulled it in the AFM (Supplementary Figure 2). Two population of unfolding steps, at 20 nm and 24 nm are detected, corresponding to the unfolding of SUMO1 and C3, respectively (Supplementary Figure 3C).

Having two marker proteins enables gating criteria that are based exclusively on the presence of the marker domains, in a manner that protein dimers can be identified and excluded from the analysis (Figure 3A,B, Supplementary Figure 8). According to experiments in which $(C3\text{-}L)_4$ and $(C3\text{-}SUMO1)_4$ are measured separately, we used the gating criterion that n(16nm) > 1 and n(20nm) = 0 marks unfolding of $(C3\text{-}L)_4$, and n(20nm) > 1 and n(16nm) = 0 defines unfolding of $(C3\text{-}SUMO1)_4$, which only misclassifies 1 out of 136 traces. Following this gating criterion, we determined the distribution of unfolding forces of C3 in the context of $(C3\text{-}SUMO1)_4$ and compared the results with C3 unfolding in the context of $(C3\text{-}L)_4$, both in TFP and OFP (Figure 3C,D). Although the mF_u of C3 in $(C3\text{-}L)_4$ appears to be 12% higher in TFP experiments (mF_u = 79.2 and 88.4 pN for the SUMO1- and L-containing heteropolyproteins, respectively),

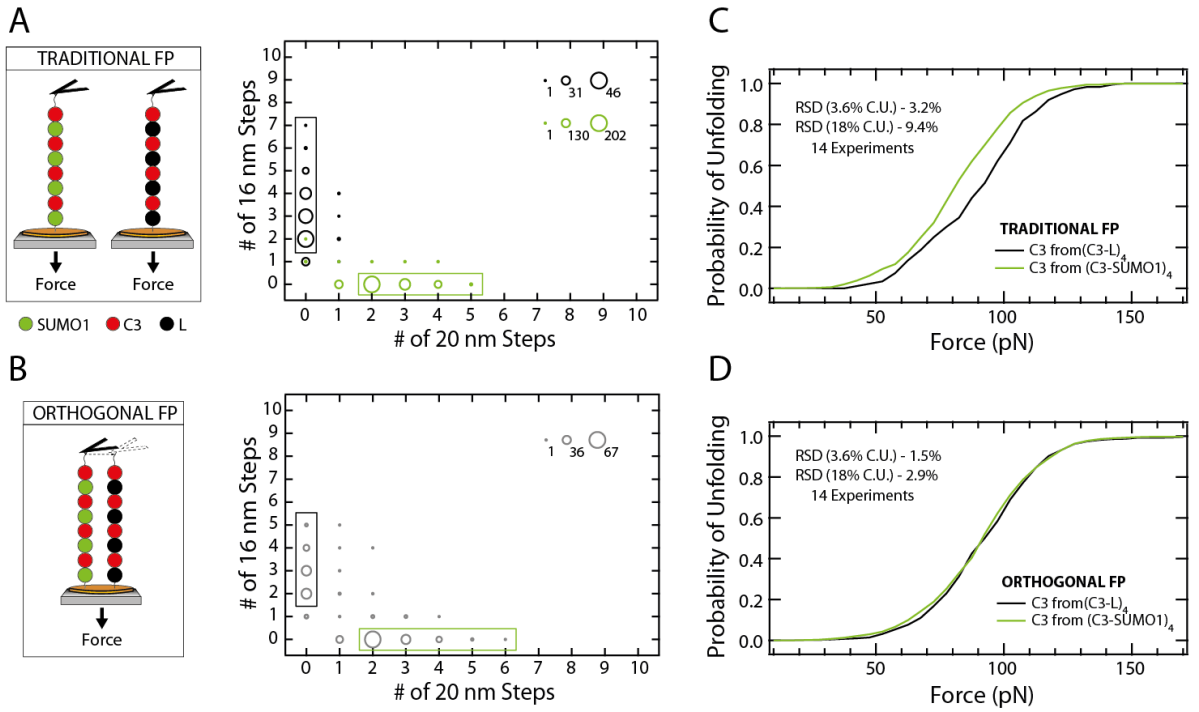

Figure 3. Dual-marker orthogonal fingerprinting overcomes confounding protein dimerization in concurrent AFM experiments. (A) Mechanical unfolding of $(C3\text{-}SUMO1)_4$ and $(C3\text{-}L)_4$ are measured in separate experiments by TFP. Individual traces are classified according to their number of 16 and 20 nm unfolding events, which mark the mechanical unfolding of protein L and SUMO1, respectively. The plot shows the frequency of the traces that have different combination of unfolding events, as indicated by the size of the dots. Traces coming from mechanical unfolding of $(C3\text{-}SUMO1)_4$ are assigned when n(16nm) = 0 and n(20nm) > 1 (green rectangle), whereas $(C3\text{-}L)_4$ events are identified by n(16nm) > 1 and n(20nm) = 0. **(B)** Mechanical unfolding of $(C3\text{-}SUMO1)_4$ and $(C3\text{-}L)_4$, as measured concurrently in OFP experiments. The plot shows the frequency of the traces that have different combination of unfolding events, as indicated by the size of the dots. The gating strategy defined in panel A allows the classification of the traces as originating from $(C3\text{-}SUMO1)_4$ (green rectangle) or $(C3\text{-}L)_4$ (black rectangle). **(C)** Experimental cumulative unfolding probability distribution of the C3 domain in the context of $(C3\text{-}L)_4$ (6 experiments, 177 events, black; data is also presented in Figure 2C) and $(C3\text{-}SUMO1)_4$ (8 experiments, 742 events, green), as measured in TFP. **(D)** Experimental cumulative unfolding probability distribution of the C3 domain in the context of $(C3\text{-}L)_4$ (873 events, black) and $(C3\text{-}SUMO1)_4$ (1043 events, green), resulting from unfolding data obtained in 14 independent OFP experiments. RSD values in the insets of panels C and D are estimated using Monte Carlo simulations that consider extreme values of calibration uncertainty (C.U.) (see also Supplementary Figure 7B). The pulling rate in all experiments was 40 pN/s.

differences vanish in OFP experiments (mF_u = 89.5 and 90.0 pN for the SUMO1- and L-containing heteropolyproteins, respectively). The RSD of the distribution of ΔmF_u, as estimated from Monte Carlo simulations fed with the actual number of experiments and events, is 2-3 times smaller in OFP than in TFP (Figure 3C,D, Supplementary Figure 7B, Supplementary Table 1)

Improvement in accuracy by balancing concurrent AFM datasets

Our Monte Carlo simulations show that the improvement in accuracy of concurrent AFM is independent of calibration uncertainty, and is preserved when multiple AFM experiments are averaged (Figure 1E,F). Here, we propose a model for the propagation of calibration errors in concurrent single-molecule AFM experiments that accounts for both observations. Considering that every unfolding force measured in the AFM is affected by an error δ, the following equation for the measured ΔmF_u can be derived (Supplementary Text 3):

$$\Delta mF_u^{measured} = \Delta mF_u^{real} + \sum_{j=1}^{n_{exp}} \bar{\delta}_j \cdot \left(\frac{n_{prot1,j}}{n_{events,prot1}} - \frac{n_{prot2,j}}{n_{events,prot2}} \right) \qquad \textit{Equation 1}$$

In Equation 1, ΔmF_u^{real} is the value of ΔmF_u that would be measured if there was no error in calibration, n_{exp} is the number of experiments, $n_{prot1,j}$ and $n_{prot2,j}$ are the number of unfolding events for both proteins being compared in concurrent experiment j, $n_{events,prot1}$ and $n_{events,prot2}$ are the total number of unfolding events for each protein considering all experiments, and $\bar{\delta}_j$ is the average value of the error in force in experiment j, which is considered to be equivalent for two proteins measured concurrently.

Equation 1 shows that in concurrent measurements, $\Delta mF_u^{measured}$ can differ from ΔmF_u^{real} according to the specific number of unfolding events obtained for each protein probed in the different AFM experiments contributing to the dataset, and to the magnitude of $\bar{\delta}_j$ values, which originate from the uncertainty in calibration. Importantly, if the proportion of events for both proteins is constant in all experiments contributing to the dataset ("balanced" condition: $n_{prot1,j} = constant \cdot n_{prot2,j}$), Equation 1 leads to $\Delta mF_u^{measured} = \Delta mF_u^{real}$, i.e. the measured unfolding force in concurrent experiments is not affected by errors in calibration, independently of the number of experiments contributing to the dataset. Our Monte Carlo simulations readily confirm this prediction. While simulations of 2 concurrent experiments with 100 events per protein show that the resulting RSD of the distribution of ΔmF_u does not depend on the uncertainty in calibration, breaking the balanced condition by considering $n_{prot1,exp1} = n_{prot2,exp2} = 150$ and $n_{prot1,exp2} = n_{prot2,exp1} = 50$, results in a dramatic increase of RSD especially at higher calibration uncertainties (Figure 4A). Under these unbalanced conditions, the performance of the concurrent strategy diminishes drastically and the obtained RSD approaches the one obtained in traditional AFM (Figure 4A).

Since unbalanced datasets result in poorer performance of concurrent AFM, we examined whether balancing datasets through data removal could result in improved accuracy. We did Monte Carlo simulations of 2 concurrent experiments in which $n_{prot1,j} = n_{prot2,j} = 50$, i.e. we trimmed 100 extra events per protein so that both experiments had the same number of unfolding events for both proteins. As expected, the RSD of the distribution of ΔmF_u after trimming becomes independent of the calibration uncertainty (Figure 4A). Even though having less events per experiment results *per se* in poorer definition of distributions of unfolding forces (Figure 1C, Supplementary Figure 5B), the RSD of the distribution of ΔmF_u obtained using trimmed datasets becomes lower than in the case of more populated, unbalanced dataset at calibration uncertainties higher than 6% (Figure 4A).

We have tested whether balancing experimental datasets also leads to improved performance of concurrent AFM. To this end, we have removed unfolding events so that every concurrent experiment verifies the balanced condition $n_{prot1} = n_{prot2}$. Using Monte Carlo simulations, we estimate that the RSD of the distribution of ΔmF_u obtained from the trimmed datasets becomes lower than the original RSD also at calibration uncertainties higher than 6-7% (Supplementary Figure 7). In the two different datasets analyzed, the differences between the balanced and the unbalanced conditions are less prominent than in Figure 4A. Indeed, we find that the extent of improvement in RSD by dataset trimming depends on the number of AFM experiments (Supplementary Figure 9). Hence, we recommend that improvement in accuracy by trimming datasets is estimated on a case-by-case basis using Monte Carlo simulations fed with actual experimental data, as we have done here.

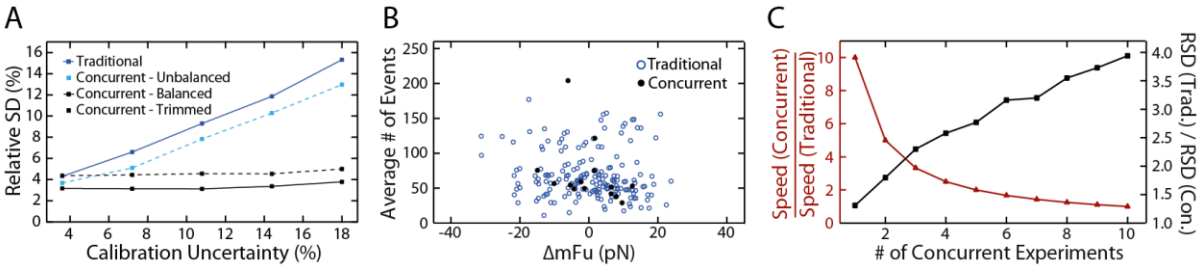

Figure 4. Improved accuracy and throughput of concurrent AFM. (A) Monte Carlo simulations show that balancing datasets obtained in concurrent AFM experiments improves RSD of distributions of ΔmF_u at calibration uncertainties >6%. Balanced simulations (solid lines, 100 events per experiment and protein) considered 2 experiments per protein in traditional (blue), and 2 experiments in concurrent AFM (black). To simulate unbalanced datasets, uneven number of unfolding events (50/150) were considered for both proteins in the first simulated experiment, and the order was reversed in the second simulated experiment (dashed blue line). The effects of balancing datasets ("trimming") was examined by running simulations at the lowest number of events for both experiments (50, dashed black line). **(B)** The experimental mF_u of C3 in the context of $(C3\text{-}L)_4$ and $(C3\text{-}SUMO1)_4$ is compared in 14 individual OFP experiments, and the corresponding ΔmF_u is represented (solid black circles). Using the same dataset, the equivalent ΔmF_u in traditional AFM was calculated from pairwise comparisons of mF_u values from different experiments (open blue circles). **(C)** Improvement in the speed of data acquisition (red) and RSD in the distribution of ΔmF_u (black) by concurrent measurements are estimated using Monte Carlo simulations at 10.8% calibration uncertainty (100 events per experiment and protein). The reference is a situation where the mF_u of two proteins are measured in 5 traditional experiments per protein.

DISCUSSION

In this report, we address a main limitation of AFM arising from uncertain calibration of cantilevers. We show that concurrent measurements result in remarkable improvements in the determination of relative mechanical properties by AFM. Prompted by our findings, we have developed widely-adaptable orthogonal fingerprinting strategies for concurrent nanomechanical profiling of proteins by AFM, leading to more accurate comparison of protein unfolding forces. Hence, OFP can define mechanical hierarchies in multidomain, elastic proteins with higher accuracy, and lead to better descriptions of the mechanical effects of mutations, posttranslational modifications and the chemical environment on proteins and their complexes [22,30-34]. Our results pave the way for similar strategies to improve mechanical characterization of cells, materials and tissues using AFM.

Concurrent AFM outperforms traditional AFM in three key aspects (Figures 4, 5):

(i) **The accuracy of concurrent AFM measurements is independent of calibration uncertainty even when multiple experiments are averaged** (Figures 1F,4A, Supplementary Figure 6). Although the uncertainty of cantilever calibration is usually considered to lie in the range of 5-25% depending on the calibration method [14], real uncertainties are extremely challenging to estimate. We have provided an experimental lower bound of 3.6% uncertainty in cantilever calibration by the commonly-used thermal fluctuations method (Supplementary Text 2). Uncertainties in spring constant calibration by the thermal fluctuations method have also been estimated by interlaboratory experiments, finding a value of up to 11% [35]. However, neither of these approaches addresses more fundamental assumptions of the calibration procedures that can lead to higher calibration uncertainties [36]. The improvements of OFP measurements with respect to traditional AFM in Figure 5 have been estimated considering a realistic calibration uncertainty of 10.8%. Due to its insensitiveness to calibration errors, concurrent AFM avoids the effects of artifacts that originate from difficult-to-detect defects in individual cantilevers, variations in the geometry of the cantilever tip that influence mechanical characterization of materials and cells [16], or changes in k_{sc} during experimentation.

Furthermore, the impact of concurrent AFM may be more relevant in the light of the advent of next generation cantilevers, which are pushing the AFM into ranges of force, stability and time resolution that are not accessible to conventional cantilevers, such in the case of high-speed AFM [37-40]. These high-performance cantilevers are more challenging to calibrate [13], so we foresee that combination of concurrent strategies and next-generation cantilevers is set to expand the reach of AFM.

(ii) **Concurrent AFM shows much improved accuracy** (Figures 1E,F, 4A,C). The increase in accuracy captured by Monte Carlo simulations is also observed in our limited experimental dataset, since the spread of ΔmF_u in pairs of OFP experiments is lower than in traditional experiments (SD = 8.0 *vs* 11.2 pN, respectively) (Figure 4B). Keeping the speed of data acquisition constant at high calibration uncertainties, the accuracy achieved by OFP measurements can be 6 times higher than in traditional AFM (Figure 5, Supplementary Figure 6B).

(iii) **The throughput of concurrent AFM is much increased**. We estimate that OFP can obtain the same accuracy in the determination of ΔmF_u over 30 times faster than traditional AFM at high calibration uncertainties (Supplementary Figure 6C). In addition, orthogonally fingerprinted proteins can be purified simultaneously (Supplementary Figures 2, 10), which results in extra savings in working time and reagents while ensuring equal experimental conditions for both proteins (Figure 5).

The increase in throughput and accuracy of concurrent AFM come at the expense of each other. Hence, depending on the goals of a particular study, the experimenter can choose to favor one or the other, or to find a balance between both. In this regard, our Monte Carlo simulations can help experimental design. For instance, in Figure 4C, we show that different gains in accuracy and throughput can be achieved depending on the number of OFP experiments carried out to compare unfolding forces of two proteins.

A direct application of our OFP data is to examine how neighboring domains affect protein nanomechanics. Indeed, the use of heteropolyproteins relies on the assumption that the effect of neighboring marker domains in the mechanics of a protein is negligible [27,41-43]. Our highly accurate OFP experiments show that the mechanical stabilities of the C3 domain in the context of a $(C3)_8$ homopolyprotein, or within a $(C3\text{-}L)_4$ or $(C3\text{-}SUMO1)_4$ heteropolyproteins, are very similar (Figures 2E, 3D). Hence, our data lend strong support to the use of heteropolyproteins in force-spectroscopy AFM. In particular, since we have shown that the mechanical properties of the C3 domain are independent of the flanking domains, the mechanical effects of mutations in C3 that cause heart disease can be directly tested using OFP strategies [44].

Mechanical characterization of proteins under the same calibration has been achieved before using microfluidics, on-chip protein expression and AFM measurements in a combined atomic force/total internal reflection fluorescence microscope [20,21]. An advantage of OFP is that it can be readily implemented in any force-spectroscopy AFM setup. In addition, different fingerprinting lengths provide additional reassurance of the identity of the probed proteins. In this regard, OFP is very well suited to compare mechanical properties of proteins with similar unfolding lengths, such as mutants of the same protein[31,34]. In those cases where proteins have different unfolding lengths, concurrent AFM measurements are of immediate application and can lead to the increase in accuracy and throughput described here. Examples include examination of the effect of disulfide bonds, protein misfolding, multimerization, and pulling geometry in the mechanical stability of proteins and their complexes [45-52], and determination of

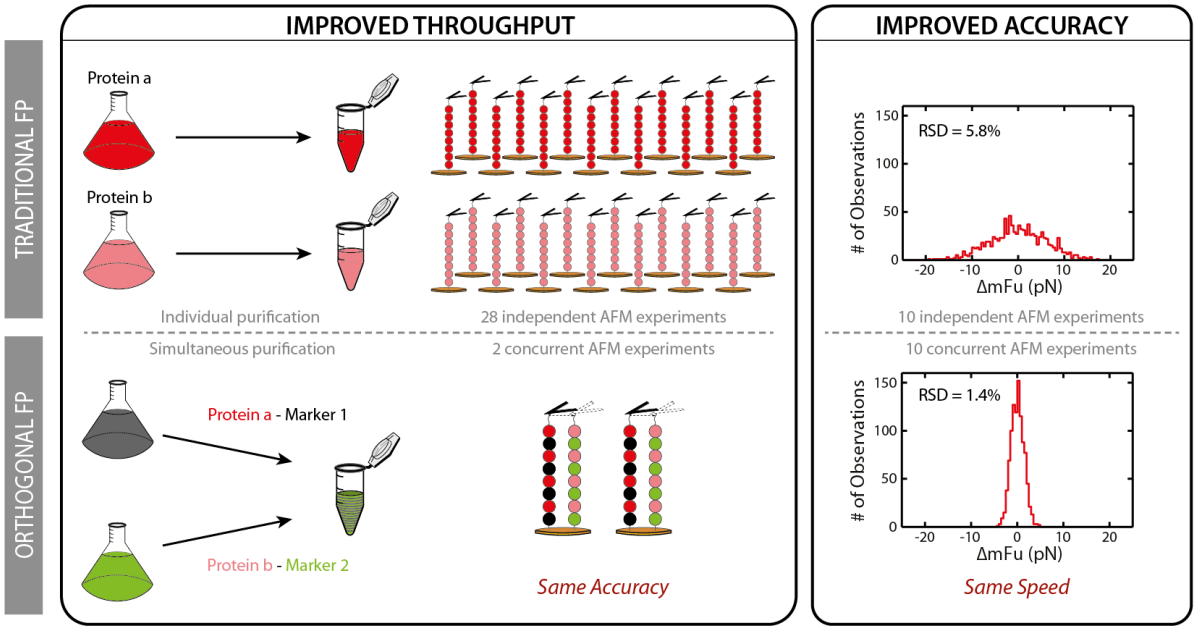

Figure 5. Overview of concurrent single-molecule force-spectroscopy AFM. In the traditional approach, comparison of the mechanical stability of *Protein a* and *Protein b* involves independent purification and several AFM experiments to compensate for inaccurate calibration of the AFM. OFP is based on the production of heteropolyproteins composed of the proteins of interest fused to marker domains. Since the markers provide unequivocal fingerprints in single-molecule pulling experiments, OFP enables simultaneous purification and concurrent measurement in the AFM, circumventing errors in force calibration. Concurrent measurements can achieve the same accuracy as conventional single-molecule AFM with much better throughput (*left*). Alternatively, by keeping the speed of data acquisition constant, concurrent AFM by OFP considerably improves the accuracy of single-molecule AFM (*right*). The improvement in throughput and accuracy are estimated from Monte Carlo simulations at 10.8% calibration uncertainty (100 events per experiment and protein).

rates of force-activated chemical reactions [53]. In these examples, our Monte Carlo simulations can be applied to guide experimental design and interpretation (code is provided as Supplementary Material).

We envision two features of OFP that will be subject of future optimization. Since the relative performance of OFP is better at high number of events (Figure 1E, Supplementary Text 4), we propose that even better accuracy can be achieved by taking advantage of high-strength single-molecule tethering strategies, which can capture more unfolding events per experiment [21,28,54]. In addition, OFP strategies hold the promise of further parallelization by the use of multiple marker proteins, which can take force-spectroscopy AFM to the realm of high-throughput single-molecule techniques [55].

METHODS

Monte Carlo simulations

Monte Carlo simulations were programmed in Igor 6 (Wavemetrics). Simulations randomly assign an error in force according to a set uncertainty in the calibration between 3.6% and 18% (Supplementary Text 2). Every simulated AFM experiment is therefore affected by a different calibration error, except under the condition of OFP, in which two proteins are measured in the same AFM experiment and share error in force. Each cycle of the simulations returns a value of ΔmF_u for two proteins using Gaussian fits to their distribution of unfolding forces, obtained from a given number of independent experiments and unfolding events. We used a bin size of 25 pN when simulating artificial datasets, or 5 pN when feeding simulations with real datasets

for better comparison with experimental distributions. Simulations calculate the RSD of the ΔmF_u distribution obtained from 1,000 cycles of the Monte Carlo procedure. RSD is defined as the SD of the distribution of ΔmF_u, normalized by the theoretical value of mF_u [23].

Distributions of unfolding forces are calculated through a kinetic Monte Carlo routine that considers that protein unfolding is exponentially dependent on force according to the Bell's model [56]:

$$r = r_0 \cdot e^{F \cdot \Delta x / k_b \cdot T} \qquad \textit{Equation 2}$$

In Equation 2, r is the rate of protein unfolding, r_0 is the rate of unfolding at zero force, F is the force experienced by the protein, Δx is the distance to the transition state, k_b is the Boltzmann constant and T is the absolute temperature. In the simulations, we considered that $k_b \cdot T$ = 4.11 pN·nm, r_0 = 0.01 $s^{-1}$and Δx = 0.2 nm. We chose these values because they are a good estimate of mechanical unfolding parameters of C3. We checked that values of RSD are fairly insensitive to small variations in r_0 and Δx and therefore one single set of parameters is enough to calculate RSD of distributions of ΔmF_u even if the mechanical parameters of the proteins to be compared are slightly different (Supplementary Table 2).

The kinetic Monte Carlo to obtain distribution of unfolding forces compares a random number with the instantaneous probability of unfolding at a given force. If the unfolding probability is higher than the random number, unfolding is considered to happen at that force. Instantaneous probabilities of unfolding are calculated following a linear approximation [57]:

$$P_u = n \cdot r_0 \cdot e^{F \cdot \varepsilon \cdot \Delta x / k_b \cdot T} \cdot \Delta t \qquad \textit{Equation 3}$$

In Equation 3, n is the number of domains that remain folded at a particular force, ε is the error in force due to the uncertain cantilever calibration (Supplementary Text 2) and Δt is the time step of the Monte Carlo. In the simulations, we used $\Delta t = 10^{-4}$ s, which ensures validity of the linear approximation, since $n \cdot r \cdot \Delta t$ is kept under 0.05 (Supplementary Text 5). Pilot simulations show that results do not vary if we use a smaller time step of 10^{-5} s.

Protein production and purification

The cDNAs coding for the C3-L and C3-SUMO1 constructs were produced by gene synthesis (NZY-Tech and Gene Art, respectively). The cDNA coding for the C3 domain was obtained by PCR. cDNAs coding for polyproteins were produced following an iterative strategy of cloning using BamHI, BglII and KpnI restriction enzymes, as described before [26,58]. Final cDNAs were inserted in the pQE80L expression plasmid using BamHI and KpnI and the resulting plasmids were verified by Sanger sequencing. Full protein sequences are reported in Supplementary Text 1. Polyproteins were expressed in BLR (DE3) *E. coli* strain. Briefly, fresh cultures (OD_{600} = 0.6-1.0) are induced with 1mM IPTG for 3 hours at 37ºC and at 250 rpm. Cells are lysed by a combination of tip sonication and passes through a French Press. Polyproteins are purified from the soluble fraction through Ni-NTA agarose chromatography (Qiagen), following the recommendations of the supplier and adding 10 mM DTT to the buffers. Further purification is achieved by size-exclusion chromatography in an AKTA Pure 25L system using a Superose 6 Increase 10/300 GL or a Superdex 200 Increase 10/300 GL column (GE Healthcare). The proteins are eluted in 10 mM Hepes, pH 7.2, 150 mM NaCl, 1 mM EDTA, which is also the

buffer used in AFM experiments. Purity of samples was evaluated using SDS-PAGE gels (a typical result is shown in Supplementary Figure 2).

Force-spectroscopy by AFM

Single-molecule AFM measurements were obtained in an AFS setup (Luigs & Neumann) according to established protocols [6].We used silicon nitride MLCT-C cantilevers with a 60-nm gold back side coating (Bruker), which we calibrated according to the thermal fluctuations method [59]. Typical spring constant values ranged between 15 and 20 pN/nm. A small aliquot (2-10 μL) of the purified protein is deposited on the surface of a gold coated cover slip (Luigs & Neumann), or directly into the Hepes buffer contained in the fluid chamber of the AFS. The cantilever is brought in contact to the surface for 1-2 s at 500-2000 pN to favor formation of single-molecule tethers. Then, the surface is retracted to achieve the set point force. If a single-molecule tether is formed, the force is increased linearly at 40 pN/s for 5 s while the length of the polyprotein is measured. This protocol ensures full unfolding of C3, L and SUMO1 domains (Supplementary Figure 3). Unfolding events are detected as increases in the length of the protein. In the initial characterization of polyproteins, we analyze all traces that contain at least two events of the same size, which allows to set a fingerprinting length for the domains (24 ± 1 nm for C3, 16 ± 1 nm for protein L, and 20 ± 1 nm for SUMO1, see Supplementary Figure 3). For the rest of the analyses, we only considered traces that contain fingerprinting unfolding lengths. Unfolding forces were recorded and plotted as cumulative distributions. mF_u values were obtained from Gaussian fits to histograms of unfolding forces. Force inaccuracy due to laser interference was lower than 40 pN in all experiments (peak-to-peak height in baseline force-extension recordings) [6].

Author contributions

J.A.C. designed the research. D.V.C engineered polyprotein constructs and produced proteins. C.P.L., C.S.C and D.S.O. did AFM experiments and analyzed single-molecule data. J.A.C programmed Monte Carlo simulations. C.P.L., C.S.C and J.A.C. run and analyzed Monte Carlo simulations and assembled display figures. J.A.C. drafted the manuscript with input from all the authors.

Acknowledgements

J.A.C. acknowledges funding from the Spanish Ministry of Economy, Industry and Competitiveness (MEIC) through grants BIO2014-54768-P, BIO2017-83640-P, and RYC-2014-16604, the European Research Area Network on Cardiovascular Diseases (ERA-CVD, MINOTAUR, AC16/00045), and the CNIC intramural grant program (03-2016 IGP). The CNIC is supported by MEIC and the Pro CNIC Foundation, and is a Severo Ochoa Center of Excellence (SEV-2015-0505). C.P.L. was a recipient of CNIC Master Fellowship. C.S.C. is the recipient of an FPI predoctoral fellowship BES-2016-076638. We thank Natalia Vicente for excellent technical support. We thank all the members of the laboratory of Molecular Mechanics of the Cardiovascular System for helpful discussions. We thank Elías Herrero-Galán (CNIC, Madrid) for critical reading of the manuscript and Lidia Prieto-Frías for key insights about propagation of calibration errors.

Competing financial interests

The authors declare no competing financial interest.

Resources

The code used for the Monte Carlo simulations is available as online Supplementary Material.

REFERENCES

1.Binnig, G. *et al.* Atomic force microscope. *Phys Rev Lett* **56**, 930-933. (1986).

2.Garcia, R. *et al.* The emergence of multifrequency force microscopy. *Nat Nanotechnol* **7**, 217-226. (2012).

3.Al-Rekabi, Z. *et al.* Multifrequency AFM reveals lipid membrane mechanical properties and the effect of cholesterol in modulating viscoelasticity. *Proceedings of the National Academy of Sciences*(2018).

4.Lai, C.-Y. *et al.* Systematic Multidimensional Quantification of Nanoscale Systems From Bimodal Atomic Force Microscopy Data. *ACS nano* **10**, 6265-6272. (2016).

5.Ando, T. *et al.* High-Speed AFM and Applications to Biomolecular Systems. *Annual review of biophysics* **42**, 393-414. (2013).

6.Popa, I. *et al.* Force dependency of biochemical reactions measured by single-molecule force-clamp spectroscopy. *Nat Protoc* **8**, 1261-1276. (2013).

7.Neuman, K. C. *et al.* Single-molecule force spectroscopy: optical tweezers, magnetic tweezers and atomic force microscopy. *Nat Methods* **5**, 491-505. (2008).

8.Rief, M. *et al.* Reversible unfolding of individual titin immunoglobulin domains by AFM. *Science* **276**, 1109-1112. (1997).

9.Linke, W. A. *et al.* Gigantic business: titin properties and function through thick and thin. *Circ Res* **114**, 1052-1068. (2014).

10.del Rio, A. *et al.* Stretching single talin rod molecules activates vinculin binding. *Science* **323**, 638-641. (2009).

11.Paluch, E. K. *et al.* Mechanotransduction: use the force(s). *BMC biology* **13**, 47. (2015).

12.Li, H. *et al.* Reverse engineering of the giant muscle protein titin. *Nature* **418**, 998-1002. (2002).

13.Slattery, A. D. *et al.* Spring constant calibration techniques for next-generation fast-scanning atomic force microscope cantilevers. *Nanotechnology* **25**, 335705. (2014).

14.Charles, A. C. *et al.* The determination of atomic force microscope cantilever spring constants via dimensional methods for nanomechanical analysis. *Nanotechnology* **16**, 1666. (2005).

15.Killgore, J. P. *et al.* Continuous measurement of atomic force microscope tip wear by contact resonance force microscopy. *Small* **7**, 1018-1022. (2011).

16.Wagner, R. *et al.* Uncertainty quantification in nanomechanical measurements using the atomic force microscope. *Nanotechnology* **22**, 455703. (2011).

17.Schillers, H. *et al.* Standardized Nanomechanical Atomic Force Microscopy Procedure (SNAP) for Measuring Soft and Biological Samples. *Scientific reports* **7**, 5117. (2017).

18.Anderson, B. R. *et al.* Single molecule force spectroscopy on titin implicates immunoglobulin domain stability as a cardiac disease mechanism. *J Biol Chem* **288**, 5303-5315. (2013).

19.Sadler, D. P. *et al.* Identification of a mechanical rheostat in the hydrophobic core of protein L. *J Mol Biol* **393**, 237-248. (2009).

20.Otten, M. *et al.* From genes to protein mechanics on a chip. *Nat Methods* **11**, 1127-1130. (2014).

21.Verdorfer, T. *et al.* Combining in Vitro and in Silico Single-Molecule Force Spectroscopy to Characterize and Tune Cellulosomal Scaffoldin Mechanics. *Journal of the American Chemical Society* **139**, 17841-17852. (2017).

22.Jobst, M. A. *et al.* Resolving dual binding conformations of cellulosome cohesin-dockerin complexes using single-molecule force spectroscopy. *eLife* **4**(2015).

23.Schlierf, M. *et al.* The unfolding kinetics of ubiquitin captured with single-molecule force-clamp techniques. *Proc Natl Acad Sci U S A* **101**, 7299-7304. (2004).

24.Alegre-Cebollada, J. *et al.* S-glutathionylation of cryptic cysteines enhances titin elasticity by blocking protein folding. *Cell* **156**, 1235-1246. (2014).

25.Carrion-Vazquez, M. *et al.* Mechanical design of proteins studied by single-molecule force spectroscopy and protein engineering. *Prog Biophys Mol Biol* **74**, 63-91. (2000).
26.Carrion-Vazquez, M. *et al.* Mechanical and chemical unfolding of a single protein: a comparison. *Proc Natl Acad Sci U S A* **96**, 3694-3699. (1999).
27.Li, H. *et al.* Multiple conformations of PEVK proteins detected by single-molecule techniques. *Proc Natl Acad Sci U S A* **98**, 10682-10686. (2001).
28.Popa, I. *et al.* Nanomechanics of HaloTag tethers. *Journal of the American Chemical Society* **135**, 12762-12771. (2013).
29.Kotamarthi, H. C. *et al.* Single-molecule studies on PolySUMO proteins reveal their mechanical flexibility. *Biophys J* **104**, 2273-2281. (2013).
30.Oroz, J. *et al.* The Y9P Variant of the Titin I27 Module: Structural Determinants of Its Revisited Nanomechanics. *Structure* **24**, 606-616. (2016).
31.Li, H. *et al.* Point mutations alter the mechanical stability of immunoglobulin modules. *Nat Struct Biol* **7**, 1117-1120. (2000).
32.Oberhauser, A. F. *et al.* The mechanical hierarchies of fibronectin observed with single-molecule AFM. *J Mol Biol* **319**, 433-447. (2002).
33.Li, H. *et al.* Atomic force microscopy reveals the mechanical design of a modular protein. *Proc Natl Acad Sci U S A* **97**, 6527-6531. (2000).
34.Williams, P. M. *et al.* Hidden complexity in the mechanical properties of titin. *Nature* **422**, 446-449. (2003).
35.te Riet, J. *et al.* Interlaboratory round robin on cantilever calibration for AFM force spectroscopy. *Ultramicroscopy* **111**, 1659-1669. (2011).
36.Ohler, B. Practical Advice on the Determination of Cantilever Spring Constants. Veeco Instruments Incorporated, Technical Report., (2007).
37.Rico, F. *et al.* High-speed force spectroscopy unfolds titin at the velocity of molecular dynamics simulations. *Science* **342**, 741-743. (2013).
38.Yu, H. *et al.* Hidden dynamics in the unfolding of individual bacteriorhodopsin proteins. *Science* **355**, 945-950. (2017).
39.He, C. *et al.* Direct Observation of the Reversible Two-State Unfolding and Refolding of an alpha/beta Protein by Single-Molecule Atomic Force Microscopy. *Angew Chem Int Ed Engl* **54**, 9921-9925. (2015).
40.Faulk, J. K. *et al.* Improved Force Spectroscopy Using Focused-Ion-Beam-Modified Cantilevers. *Methods Enzymol* **582**, 321-351. (2017).
41.Dietz, H. *et al.* Exploring the energy landscape of GFP by single-molecule mechanical experiments. *Proc Natl Acad Sci U S A* **101**, 16192-16197. (2004).
42.Steward, A. *et al.* Versatile cloning system for construction of multimeric proteins for use in atomic force microscopy. *Protein Science* **11**, 2179-2183. (2002).
43.Oroz, J. *et al.* Unequivocal Single-Molecule Force Spectroscopy of Proteins by AFM Using pFS Vectors. *Biophys J* **102**, 682-690. (2012).
44.Harris, S. P. *et al.* In the thick of it: HCM-causing mutations in myosin binding proteins of the thick filament. *Circ Res* **108**, 751-764. (2011).
45.Giganti, D. *et al.* Disulfide isomerization reactions in titin immunoglobulin domains enable a mode of protein elasticity. *Nat Commun* **9**, 185. (2018).
46.Manteca, A. *et al.* Mechanochemical evolution of the giant muscle protein titin as inferred from resurrected proteins. *Nat Struct Mol Biol* **24**, 652-657. (2017).
47.Manteca, A. *et al.* The influence of disulfide bonds on the mechanical stability of proteins is context dependent. *J Biol Chem* **292**, 13374-13380. (2017).
48.Bertz, M. *et al.* Mechanical stability of the antibody domain CH3 homodimer in different oxidation states. *J Am Chem Soc* **135**, 15085-15091. (2013).
49.Carrion-Vazquez, M. *et al.* The mechanical stability of ubiquitin is linkage dependent. *Nat Struct Biol* **10**, 738-743. (2003).

50. Oberhauser, A. F. *et al.* Single protein misfolding events captured by atomic force microscopy. *Nat Struct Biol* **6**, 1025-1028. (1999).
51. Sarkar, A. *et al.* The mechanical fingerprint of a parallel polyprotein dimer. *Biophys J* **92**, L36-38. (2007).
52. Carl, P. *et al.* Forced unfolding modulated by disulfide bonds in the Ig domains of a cell adhesion molecule. *Proc Natl Acad Sci U S A* **98**, 1565-1570. (2001).
53. Garcia-Manyes, S. *et al.* Force-activated reactivity switch in a bimolecular chemical reaction. *Nat Chem* **1**, 236-242. (2009).
54. Zakeri, B. *et al.* Peptide tag forming a rapid covalent bond to a protein, through engineering a bacterial adhesin. *Proc Natl Acad Sci U S A* **109**, E690-697. (2012).
55. Hill, F. R. *et al.* The more the merrier: high-throughput single-molecule techniques. *Biochemical Society transactions* **45**, 759-769. (2017).
56. Bell, G. I. Models for the specific adhesion of cells to cells. *Science* **200**, 618-627. (1978).
57. Shi, J. *et al.* Simulated data sets for single molecule kinetics: some limitations and complications of data analysis. *European biophysics journal : EBJ* **35**, 633-645. (2006).
58. Alegre-Cebollada, J. *et al.* Isopeptide bonds block the mechanical extension of pili in pathogenic Streptococcus pyogenes. *J Biol Chem* **285**, 11235-11242. (2010).
59. Hutter, J. L. *et al.* Calibration of atomic-force microscope tips. *Review of Scientific Instruments* **64**, 1868-1873. (1993).